Journal of Energy Storage 51 (2022) 104526

Contents lists available at ScienceDirect

Journal of Energy Storage

journal homepage: www.elsevier.com/locate/est

Research papers

Binary composite (TiO_2-Gr) based nano-enhanced organic phase change material: Effect on thermophysical properties

Imtiaz Ali Laghari [a], M. Samykano [a,*], A.K. Pandey [b,c,**], K. Kadirgama [d], Yogeshwar Nath Mishra [e]

[a] College of Engineering, University Malaysia Pahang, Lebuhraya Tun Razak, 26300 Gambang, Kuantan, Pahang, Malaysia
[b] Research Centre for Nano-Materials and Energy Technology (RCNMET), School of Engineering and Technology, Sunway University, No. 5, Jalan Universiti, Bandar Sunway, Petaling Jaya, 47500, Selangor Darul Ehsan, Malaysia
[c] Center for Transdisciplinary Research (CFTR), Saveetha Institute of Medical and Technical Sciences, Saveetha University, Chennai, India
[d] Faculty of Mechanical & Automotive Engineering Technology, Universiti Malaysia Pahang, 26600 Pekan, Pahang, Malaysia
[e] NASA-Jet Propulsion Laboratory, California Institute of Technology, California 91109, USA

ARTICLE INFO

Keywords:
Paraffin wax
Binary nanocomposite
Phase change materials
Thermal energy storage

ABSTRACT

The latent heat storage technology using Phase Change Materials (PCMs) has recently been extensively utilized in energy conservation and management to reduce energy consumption. To improve the thermal conductivity of PCMs, they have been incorporated with nanoparticles. In this article, we report, Titanium dioxide-Graphene (TiO_2:Gr) binary composite (1 wt% TiO_2: 0.1, 0.5, 1 and 2 wt% of Graphene (Gr)) with Paraffin wax (PW) to improve the thermophysical properties added with sodium dodecylbenzene sulphonate (SDBS) as surfactant. Ultraviolet-visible spectrometer (UV–VIS), Fourier transform infrared spectroscopy (FT-IR), Differential scanning calorimeter (DSC), Thermogravimetric analyzer (TGA), Field Emission Scanning Electron Microscopy (FESEM) and Thermal property analyzer (TEMPOS) were used for material characterizations. The latent heat capacity of the PW/Titanium oxide (TiO_2) composite and the PW/TiO_2-Gr binary composites were improved by 8.62% and 10.02%, respectively, in comparison to base PCM. The thermal conductivity of the composite PCMs with PW/TiO_2-1.0 and PW/TiO_2Gr-1.0 is 120% and 179% higher than base PW. The FT-IR spectra demonstrated no chemical interaction between the PW and the nanoparticles. TGA results presented improved thermal stability by integration of the TiO_2-Graphene particles into the matrix of paraffin wax. The light transmission of the prepared composite was reduced by 58.30% related to base PW, resulted increased light absorption and, subsequently, enhanced photothermal conversion. The composite's improved thermal conductivity and enthalpy make it a strong contender for use in TES and solar photovoltaics thermal systems.

1. Introduction

Energy security and climate change are the two most critical issues in the world today, and they are intimately connected. On the one hand, today's global energy system is mainly reliant on conventional fossil fuels, which are rapidly depleting; however, the emissions from using this fuel constitute a significant contributor to climate change [1,2]. Using surplus heat from solar and other energy sources, thermal energy storage systems (TES) developed one of the required means for dropping dependence on fossil fuel and leading to more effective and environmentally sustainable energy storage [3]. Phase change materials (PCM's) recommended as possible energy storage mediums have gotten much attention recently. When PCM absorb and release significant quantities of latent heat storage (LHS) during phase change, the technology allows for storage, transportation and use of thermal energy. The PCM can be classified as Organic, Inorganic and Eutectics based on material properties. Organic PCMs have become standard for energy storage in recent years due to their high thermal stability. Some PCMs have a higher energy density, which means they can store and release a tremendous amount of energy [4]. However, some issues with PCM's, such as low thermal conductivity (TC) and lower thermophysical properties (TPP), will arise in use. It is essential to integrate nanoparticles into PCMs to enhance their TC [5]. Additionally, nanoparticles could increase the

* Corresponding author.
** Correspondence to: A.K. Pandey, Research Centre for Nano-Materials and Energy Technology (RCNMET), School of Engineering and Technology, Sunway University, No. 5, Jalan Universiti, Bandar Sunway, Petaling Jaya, 47500, Selangor Darul Ehsan, Malaysia.
E-mail addresses: mahendran@ump.edu.my (M. Samykano), adarsh.889@gmail.com (A.K. Pandey).

https://doi.org/10.1016/j.est.2022.104526
Received 1 November 2021; Received in revised form 11 March 2022; Accepted 23 March 2022

Nomenclature

CuO	Copper oxide nanoparticles
DSC	Differential scanning calorimetric
EDX	Energy-dispersive X-ray spectroscopy
FESEM	Field emission scanning electron microscope
FT-IR	Fourier transform infrared spectroscopy
Gr	Graphene nanoparticles
LHS	Latent heat storage
MWCNT	Multi-wall carbon nanotubes
NEOPCM	Nano-enhanced organic Phase change materials
NEPCM	Nano-enhanced phase change materials
PCM	Phase change materials
PV	Photovoltaics
PVT	Photovoltaic thermal systems
PW	Paraffin wax
PW/TiO_2	Paraffin titanium oxide composite
PW/TiO_2Gr	Paraffin Titanium oxide-Graphene binary composite
SST	solid to solid transition
SLT	solid to liquid transition
SDBS	Sodium dodecylbenzene sulphate
SA	steric acid
TC	Thermal conductivity
TGA	Thermal gravimetric analyzer
TiO_2	Titanium oxide
TPP	Thermo-physical properties
UV–VIS	Ultra-violet visible spectroscopy

Greek letters

α	Absorptance
β	Temperature coefficient
ρ	Density kg/m^3
η	Efficiency
H	Photovoltaic efficiency
μ	Micron
ϕ	Concentration ratios (%)

surface area to volume ratio and decrease the solidification and melting rate.

High conductive nanoparticles dispersed in the PCM offer a promising solution for improving TC and sustaining thermal efficiency [6]. Therefore, Nano-enhanced organic phase change materials (NEOPCM's) have been found to be some of the most promising energy storage materials, surpassing the limitations of PCM's [7–9]. The TC of NEOPCM is influenced by nanoparticles' inherent TC and the PCMs and nanoparticles interactional compatibility [10]. Carbon-based nanotechnology such as carbon nanotubes, oxides and metallic nanoparticles have already been used in heat transfer products, which can be combined to increase their performance [11], for example, using dispersants with PCMs to improve (TC) and heat transfer [12]. Due to their lower energy charge/discharge ratios, the need for the PCM to improve their TC's is obvious [13]. Therefore, nanoparticles that improve their TCs or that help influence composite PCMs are being sought to generate high energy charging/discharging speed.

Paraffin with polyaniline nanocomposite was created by dispersion with simple sonification [14]. The improved dispersion of conducting polymers-based nanocomposite gave a 15.9% increase in LHS. The PCM will store additional thermal energy when the latent heat is increased. The TC improved by 20.4% resulted increases charging performance because decreased interfacial resistance results in increased efficacy of PCM. The thermal energy storage study was directed for thermal efficiency using carboxyl functionalize Graphene doped with paraffin wax (PW) [15]. Volume concentrations were increased by 0.25 to 1%. By using doped PCM materials, it was observed that an enhancement in TC result increased the charging time decrease rate up to 20.0% to 30.0% due to variation in HTF inlet temperature. When the charging time was decreased by 30% to 50% using 1% composite in Paraffin, a considerable quantity of energy was stored concisely. The carbon nanoparticles combined with graphite speed up the solidification process [16]. The melting process for the nano enhanced PCM was increased by 21% as related to PW, while the composition of carbon foam/PW improved by 31%. That being said a 42% increase in TC for the composite PCM. The reported work [17] demonstrated that expanded graphite (EG)-paraffin wax composite PCMs solar absorption capacity increased by introducing small quantity of carbon nanotubes (CNTs) as the light absorbent. The produced composite PCMs containing 5% EG and 2% CNTs exhibit exceptional thermal conductivity a high solar absorption capacity, and a high latent heat capacity. Additionally, these enhanced thermal and optical characteristics are stable after 1000 melting-freezing cycles. Paraffin with reduced graphene oxide and zirconium carbide was created for enhanced light transmission and thermophysical properties [18]. The composites PCMs with varying amounts of zirconium carbide exhibited outstanding photo absorption, thermal storage capacity, and heat transmission properties. When doped with 0.01 wt% zirconium carbide, the photothermal conversion efficiency increases to 81%. Composite PCMs found to be maximum thermal conductivity of 121% greater than PW. Chen et al. [19] examined the impact of CuO nanoparticles' light absorption capabilities on PW. The composites were prepared with a mass fraction of CuO varying from 0.01 to 0.1%, and found that the composites increased the steady state temperature by 2.3 times. The ability to absorb light was increased when the mass fraction of CuO nanoparticles increased. A novel method was used to make a nanoparticle enhanced PCM stearic acid SA TiO_2 [20]. The finding showed they had higher TC values compared with base PCM. NEPCM composite was made with weight concentration 0.09, 0.26, 0.33 and 0.36 wt percentage. The highest TC was reported as 27% compared with pure SA PCM. The work reported is directly associated with using different combinations of Al_2O_3-CuO hybrid nanoparticles (75:25, 50:50 and 25:75) [21]. These hybrid nanoparticle combinations were integrated with varied volume concentrations of 0.5, 1, 2, and 3% and then subjected to TC and melting point tests utilizing the KD-2 Pro and digital melting point equipment, respectively. The inclusion of hybrid nanoparticles improved the TC and melting temperature (MT) of the PCM composite, according to the study's findings. Sun et al. [22] characterized the TPP of PW and nanocarbon materials. The paraffin/nanocarbon of three different samples, 0.02, 0.06 and 0.10%, were characterized. The highest increment in NEPCM TC was found at 0.06, and 0.10% were 25% and 12%, respectively. It was also pointed out that the 20% decrease in the melting temperature by adding nanocarbon to Paraffin PCM. Paraffin were doped at the level of 0, 0.5, 1.0, 1.5 and 2.0% with TiO_2 to improve thermal response [23]. Results demonstrated improved results of latent heat as compared with paraffin LHS. The increment in the TC values 33, 66, 84 and 101% was also seen by adding the TiO_2 concentration without disturbing the chemical edifice. Binary Graphene-Silver (Gr-Ag) nanomaterial used for the first time with PW PCM to improve its TPP [24]. By 0.3% of binary Gr-Ag nanomaterial loaded in PCM, the most significant increase in TC as well as the improvement in LHS was around 40% noticed. The examination of the thermal performance of solid-solid PCM with binary composite and multi-nanoparticles addition composite was evaluated by [25]. The thermal behavior of improved neopentyl glycol (NPG) composites has been reported and discussed in various cases. It was found that the influence of the element concentration ratio in a multi nanoparticles combination on the thermal performance of NPG. SiO_2, Al, and TiO_2 had higher TC and LHS.

While numerous studies have focused on preparing NEPCM with increased TC of composites, none of them had addressed the TiO_2 and Graphene binary combination to prepare PW-TiO_2Gr composite. The novelty lies in the fact that the paraffin TiO_2-Graphene is the first time to the authors knowledge that composite can be made in the current study. This study aims to investigate the impact of TiO_2-Graphene for energy storage application on the TPP of the paraffin RT47. According to the literature review, TC and LHS of composites are critical when it comes to using energy storage. The TC allows heat from the materials to go through the PCM more quickly while LHS is the quantity of energy it can hold before it overheats significantly. Therefore, we have performed a comprehensive characterization of the materials in this study using techniques such as FESEM, EDX, FTIR, UV–Vis, and TGA. This allows for a detailed analysis of their morphological, chemical compatibility, thermal stability and other properties. Further, a wide temperature range is included in medium temperature-based applications using the produced material, such as cooling of PV (40 °C–70 °C), PVT (40 °C–90 °C) [26,27], electronic devices (40 °C–80 °C) [28], automotive battery cooling (37 °C–67 °C) [29], hot water application (40–65 °C).

2. Materials and methods

2.1. Materials

Paraffin RT47 Organic PCM with a melting point around 47–48 °C and excellent phase change enthalpy of 160 kJ/kg is obtained from RUBITHERM ®Germany. TiO_2 nanoparticles having particles size of 25 nm purchased from Sigma-Aldrich Company and Graphene nanoparticles 8 nm-sized obtained from Graphene Supermarket. Surfactant SDBS was purchased from Sigma-Aldrich company Germany. The physiochemical properties of the materials used are listed in Table 1.

2.2. Preparation of NEOPCM and binary NEOPCM

A two-step technique achieved the preparation of TiO_2-Graphene binary nanoparticles dispersed in RT47 Paraffin organic PCM, as seen in Fig. 1. The appropriate weight of base PCM, TiO_2 nanoparticles, and SDBS surfactant (0.1%, 0.5%, 1%, and 2%) measured by analytical microbalance. Paraffin RT47 PCM was melted at 70 °C by using a hotplate (RCT, BASIC IKA), then TiO_2 nanoparticles and SDBS was added with melted base PCM and sonicated for 30 min by using probe-sonicator (Model; FS-1200N) for proper mixing of composite.

The composite was permissible to cool at ambient temperature. The same method is used to make binary composites NEOPCM Paraffin/TiO_2-Graphene (PW/TiO_2Gr). The composite 1.0-PW/TiO_2 was melted at 70 °C by using a hotplate (RCT BASIC IKA). Graphene nanoparticle was added at a different wt per cent (0.1%, 0.5%, 1% and 2%). Probe sonication has been done for proper mixing of NEOPCM binary composite. Then it was allowed to let the composition reach room temperature. The various concentrations of RT47 PW with TiO_2 are represented as PW, PW/TiO_2-0.1, PW/TiO_2-0.5, PW/TiO_2-1.0, and PW/TiO_2-2.0 for weight concentrations of TiO_2 at 0%, 0.10%, 0.50%, 1.0%, and 2.0%, correspondingly. Likewise, binary composites comprising RT47-TiO_2 added Graphene are signified as PW/TiO_2Gr-0.1, PW/TiO_2Gr-0.5, PW/TiO_2Gr-1.0, and PW/TiO_2Gr-2.0 for Graphene weight concentrations of 0.1, 0.5, 1%, and 2.0%.

Table 1
Physiochemical properties of PW RT-47 PCM (47–48 °C).

Properties	
PCM	RT47
Class	Organic ester PCM
Latent heat capacity	160 kJ/kg
Thermal conductivity	0.20 W/m/K
Colour	Bluish-white
Density	0.88 kJ/l (solid) 0.77 kJ/l (liquid)
Solubility	Insoluble in water

2.3. Characterization methods

To investigate the morphological, chemical, and thermal characteristics of NEOPCM, a variety of facilities were utilized. The morphology of the PW base, PW/TiO_2 and (PW/TiO_2-Graphene) composite was studied with the help of Field Emission Scanning Electron Microscopy (FE SEM). The scanning electron microscope was equipped with an Energy Dispersive X-ray Spectroscopy (EDX) system, which was utilized to determine the elemental compositions of the samples directly. An FTIR technique with a wavenumber range of 400–4000 cm^{-1}, a spectral resolution of 0.1 cm^{-1}, and a wave number precision of 0.01 cm^{-1} were used to determine the chemical compositions and functional groups. The ATR-RX1 spectrometer was used to create comprehensive FT-IR spectra curves in transmittance mode. Under an N_2 environment and at a heating rate of 10 °C/min, composites' mass loss and thermal stability anticipated using the Thermal gravimetric analyzer (TGA 400 Perkin Elmer 4000). The LHS and MP of material properties were measured using a DSC-1000 M (Linseis Inc., (USA)). The DSC equipment was calibrated with the help of the Linseis TA software. We conducted a TC test on NEOPCM (PW/TiO_2 and PW/TiO_2Gr) utilizing a TEMPOS dual needle SH3 sensor Thermal analyzer, which measured TC. Optical absorbance measurement was performed using UV–Vis' spectroscopy (LAMBDA 1050, Perkin Elmer, USA). The measurements are taken at room temperature and in the wavelength range 200–800 nm.

3. Results and discussion

3.1. Morphological characterization of NEOPCM and binary NEOPCM

The morphological analysis for TiO_2 nanoparticles, Graphene nanoparticles, base PW, nanocomposite (1.0-PW/TiO_2) with 1% TiO_2 relative to paraffin wax and binary composite (1.0-PW/TiO_2Gr) was carried out, and FESEM images are shown in Fig. 2. According to Fig. 2(a), TiO_2 nanoparticles may be readily observed at a magnification of 150 times the standard magnification. The diameter of these nanotubes ranges from 20 to 40 nm, and their surface is porous. The size of Graphene nano powder is below 10 nm, FESEM analysis of Graphene nanoparticles demonstrated a flakes-like structure, as illustrated in Fig. 2(b). The FESEM of pure PW is presented in Fig. 2(c), which only reveals a lamellar layered structure and no other features. When paraffin wax is doped with TiO_2 and binary TiO_2-Graphene, it can be seen in Fig. 2(d) and (e), the wax's smooth surface become uneven, revealing pores and particles contained in the matrix—TiO_2 functions as an irregular particle uniformly distributed over the Graphene surface [30]. Even though TiO_2 is larger than graphene nano powder, high magnification of the composite material is not possible as the material starts to melt as the magnification increases. The elemental mapping of the sample is shown as evidence of the presence of TiO_2. However, as Carbon is the element for paraffin wax and graphene, to distinguish the presence of graphene from paraffin wax is not possible through elemental mapping. Another difficulty in identifying graphene nano powder is the layer-by-layer structure as evident in SEM image. Therefore, during the preparation of the composite, the graphene layers may have been embedded on the waxy structure of paraffin wax leading to difficulty in recognizing graphene from paraffin wax. However, TiO_2 is clearly seen from the change in smooth surface to small round uneven surface from the addition of titanium dioxide (Fig. 2e).

Nevertheless, it can be viewed in Fig. 2(e) that TiO_2 has grown on the surface of the Graphene. It is because of the functional groups on the Graphene surface, which act as anchoring sites while inhibiting nanoparticles agglomeration [30,31]. Consequently, the FESEM examination of the nanocomposite reveals that the TiO_2-Graphene particles have

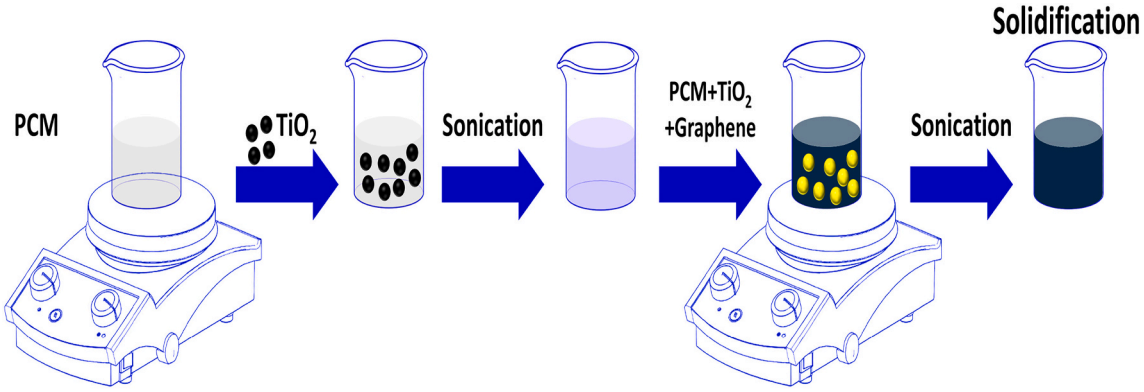

Fig. 1. Preparation of binary NEOPCM composite.

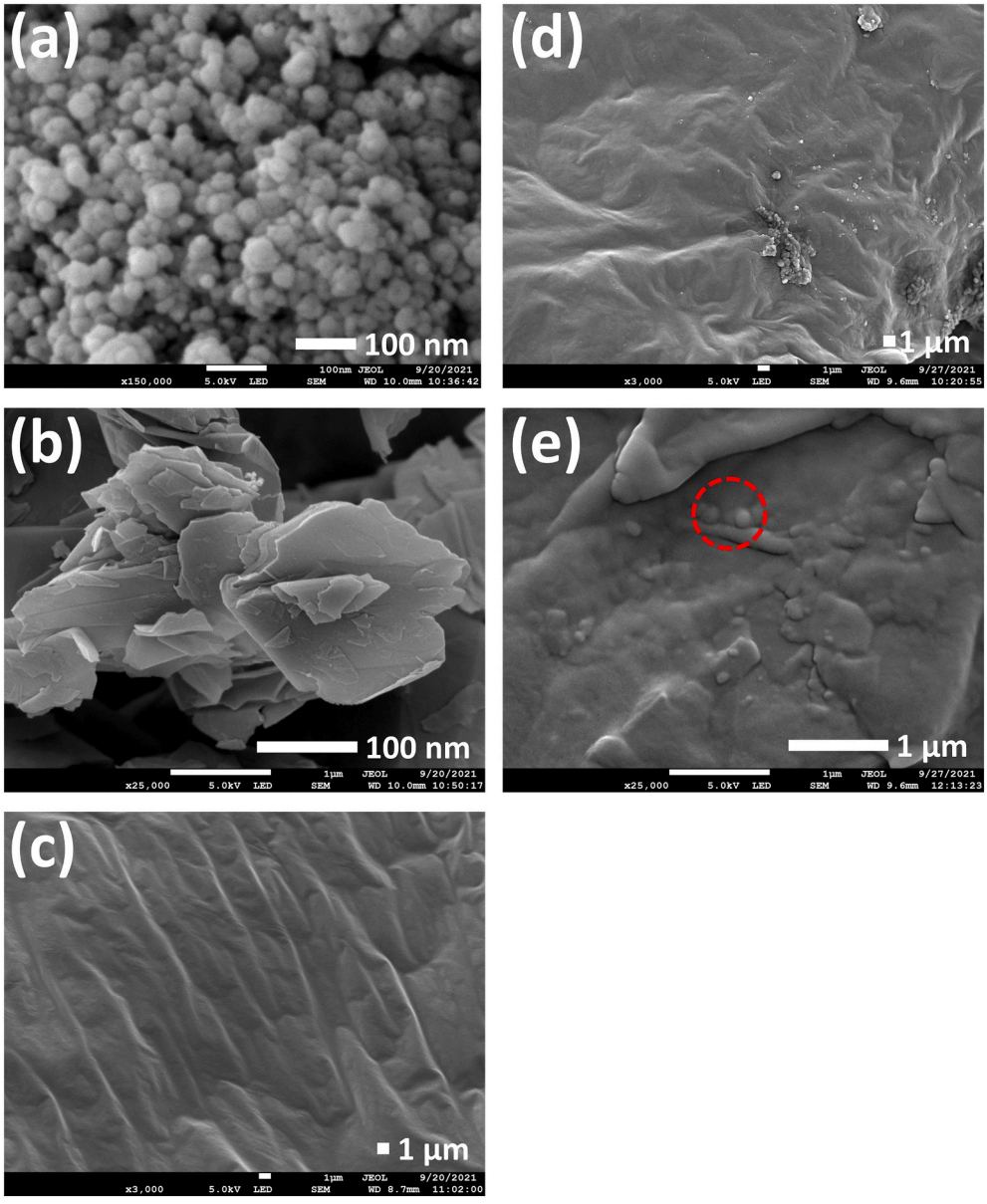

Fig. 2. FESEM images (a) TiO_2 nano particles. (b) Graphene nano particles. (c) Paraffin wax RT47. (d) PW/TiO_2 composite. (e) PW/TiO_2 graphene binary composite.

been integrated into the matrix of paraffin wax.

The element mapping approach is beneficial for visualizing element distributions; it was selected to produce a more accurate representation of the dopant's dispersion in PW. Paraffin/TiO_2 nanocomposite mapping is shown in Fig. 3, and PW/TiO_2-Graphene composite element mapping is shown in Fig. 4. From the figures, it is seen that the dopant has been evenly disseminated throughout the paraffin matrix. Fig. 3 shows the EDX spectrum's peaks of the elements such as C, O, Ti, Na, Ag, and Zr. Additionally, the weight per cent of C, O, Na, Mg, S, Ti, and Zr in the 1.0-PW/TiO_2 nanocomposite was 77.59, 7.45, 0.69, 9.59, 1.83, 1.09, and 10.75, respectively. Similarly, Fig. 4 shows the elemental structure and elements of the PW/TiO_2 Gr nanocomposite. The weight percentages of C, Na, S, and Ti in the 1.0-PW/TiO_2Gr nanocomposite were determined to be 90.83, 6.35, 0.37, 0.63, and 1.82%, respectively.

3.2. Latent heat storage

Fig. 5 a shows enthalpy outcome with different mass fractions of PW/TiO_2 composite and pure PW RT 47. The base PCM supplier's data shows that the enthalpy, melting and solidifying temperature of base PW PCM and nanocomposite materials are slightly less. All the prepared nanocomposites presented an enhancement in the LHS except 1.0-PW/TiO_2 and 2.0-PW/TiO_2. When the loading exceeds 1%, the LHS decrease below those of the base PW, due to two opposing factors cause changes in the composite's LHS. 1) The LHS of the composites increases due to the interaction of PW molecules and TiO_2 particles, and 2) the LHS decreases by the addition of TiO_2 particles because nanoparticles may absorb or release more energy during the composite melting or solidification processes. Thus, if the first component is more vital than the second, the composite's LHS enhances, and vice versa [32]. The downward trend of the initial peak shows the change of phase from solid to liquid. PW and PW/TiO_2 composites show solid-solid transition (SST) in the range of 30 °C–40 °C temperature. In comparison to the solid-liquid transition (SLT), the solid-to-solid peak is smaller. The SST occurs when the molecular structure changes from ordered to disordered. The second peak corresponds to the phase change from solid to liquid. As can be observed, the phase change begins at around 30 °C and finishes at approximately 80 °C. The area beneath the phase transition peaks of PW and PW/TiO_2 composites is used to determine the total LHS. The melting point is determined by finding a tangent on the left slope that passes through the DSC curve's apex.

The lower curve depicts the melting processes of the composites; it indicates that adding TiO_2 nanoparticles has little effect on the melting point of paraffin wax. The melting point has been increased by 47 °C to 50 °C by adding TiO_2 nanoparticles. The appropriate enthalpies were determined by integrating the peaks over the DSC software's baseline. As seen in this figure, the melting and crystallization enthalpies of paraffin nanocomposites with a mass fraction of 0.1% are pretty higher than those of pure wax. The Van der Waals interactions between the TiO_2 nanoparticles and the PW are responsible for this latent heat increase [33]. The heat absorbed during the solid-to-liquid transition is utilized to overcome the PCM's weak intermolecular forces. If the particle concentration is high enough, the presence of nanoparticles can change these forces so that the interaction potential between the paraffin wax and the nanoparticles is greater than the interaction potential between the wax molecules themselves. Due to the nanoparticles' exceptionally high surface to volume ratio, a low concentration of them can improve molecular interaction and raise the latent heat of the nanocomposites. The latent temperatures of fusion of NEOPCM are deteriorated at increasing concentrations due to the accumulative replacement of paraffin wax by nanoparticles.

The highest LHS enhancement was seen for the composite 0.1-PW/TiO_2 at 7.98% 157.0 ± 3.14 J/g and melting temperature 46.20 ± 0.2 °C, 1% enhancement in the LHS recorded for the composite 0.5-PW/TiO_2 at 146.30 ± 2.92 J/g. All the results of latent heat capacity for 0.1-PW/TiO_2, 0.5-PW/TiO_2, 1.0-PW/TiO_2 and 2.0-PW/TiO_2 are 1%, 7.98%, −16% and −15% respectively as can be seen in Fig. 5(a). The melting point of all composites is essentially the same as the base PW. However, except 2.0 PW/TiO_2, all composites exhibit a decrease in melting temperature compared to pure PW. It can be explained by the nature of the interaction between the composite's components. TiO_2 nanoparticles have a high surface area, and the intermolecular interaction between the molecules in the PW/TiO_2 dispersion might account for the increase in latent heat energy [34]. The shift in melting temperature was caused by the weak attractive contact between the fluid and the matrix surface [35].

Fig. 5(b) shows enthalpy outcome with different mass fractions of PW/TiO_2Gr composite. Except for PW/TiO_2Gr-1.0, PW/TiO_2Gr-2.0, every produced nanocomposite shown an increase in latent heat capacity, as illustrated in Fig. 5(b). The downward trend of the first peak indicates the transition from the solid to the liquid phase. PW and PW/TiO_2Gr composites have an SST temperature range of 30 °C–40 °C. The SST has a smaller peak than the solid-liquid transition. When the molecular structure shifts from organized to disordered, the solid-to-solid transition occurs. The second peak indicates the phase transition from solid to liquid. As evidenced by the preceding, the phase transition begins at about 30 °C and ends around 80 °C. Total latent heat is calculated by measuring the area beneath the phase transition peaks of PW and PW/TiO_2Gr composites. The melting point is calculated by locating a tangent on the left slope that crosses through the peak of the DSC curve. The highest enhancement was 10.02% for the composite 0.1-PW/TiO_2Gr, a latent heat capacity of 160.0 ± 3.20 J/g and a melting temperature of 49.12 ± 0.2 °C, 4.74%. The LHS capacity of 0.1-PW/TiO_2, 0.5-PW/TiO_2Gr, 1.0-PW/TiO_2Gr, and 2.0-PW/TiO_2Gr are 160.0 ± 3.20 J/g, 158 ± 3.16 J/g, 130.04 ± 2.60 J/g and 122 ± 2.44 J/g. All composites have a melting point that is nearly identical to that of the base PW. However, all composites, except for 1.0 PW/TiO_2Gr and 2.0 PW/TiO_2Gr, have a lower melting point than base PW. It can be explained by

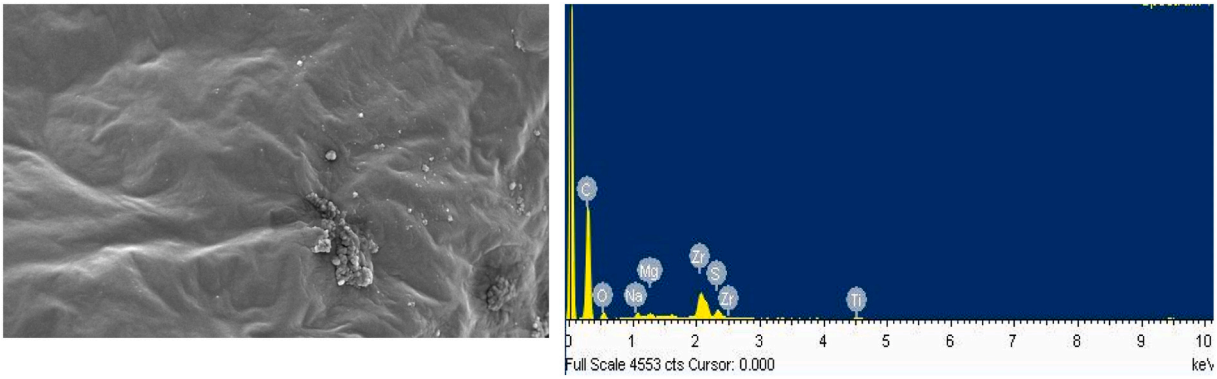

Fig. 3. The element mapping PW/TiO_2 composite. Left image: showing the elemental mapping. Right image: elements and their weight percentage.

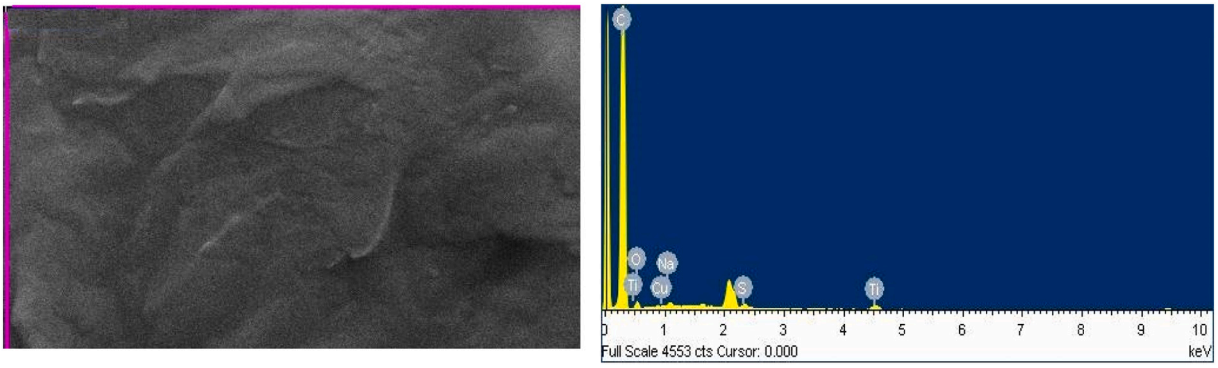

Fig. 4. Element mapping of PW/TiO_2 graphene binary composite. Left image: showing the elemental mapping. Right image: elements and their weight percentage.

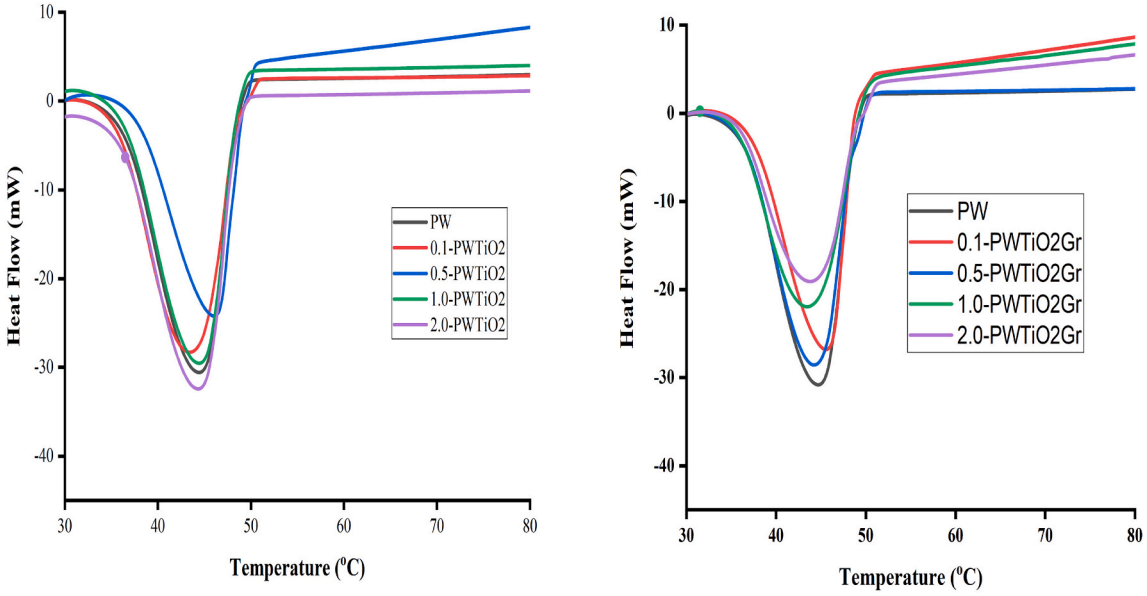

Fig. 5. DSC Curve of heat flow vs temperature (a) PW-TiO_2 (b) PW-TiO_2 Gr.

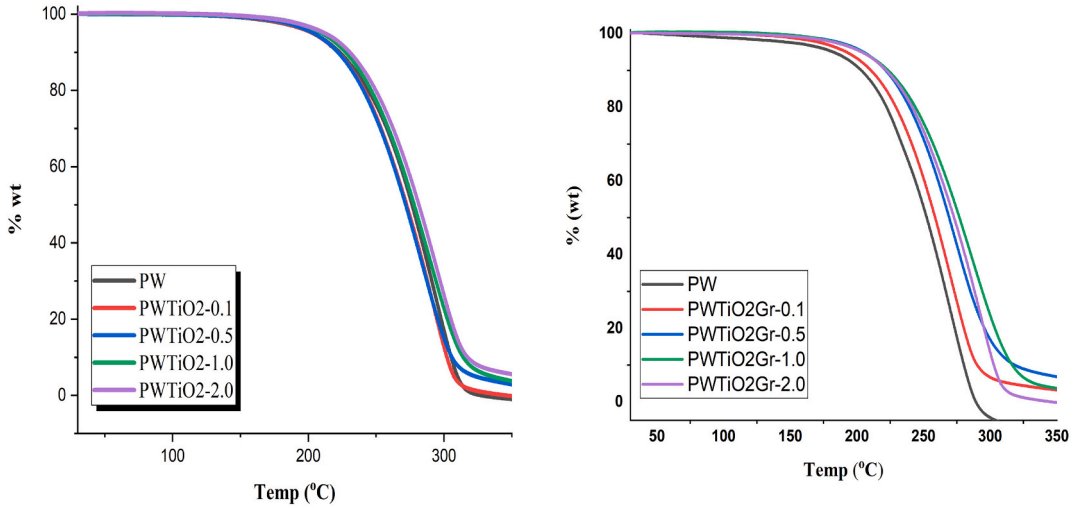

Fig. 6. TGA curve of weight % vs temperature for PW/TiO_2 in (a) and for PW/TiO_2Gr in (b).

the way the composite's components interact. The shift in melting temperature might have been induced by the fluid's weak attractive interaction with the matrix surface. TiO_2-Graphene nanoparticles have a high surface area, and the intermolecular interaction between the molecules in the PW/TiO_2Gr dispersion might account for the increase in latent heat energy.

3.3. Thermal stability

In various concentrations, the thermogravimetric analyzer (TGA) evaluates the durability of the prepared composites PW/TiO_2 and PW/TiO_2Gr added Graphene are presented in Fig. 6a and b respectively. TGA measures are performed to ensure the precision of results obtained using a mass value of 10 mg and a heating rate of 10 °C/min in the 450-temperature range. Weight deterioration over temperature is illustrated in the Fig. 6; the downward trend indicates that the weight loss arises for PW and PW/TiO_2 composites. The increase in nanoparticle concentration enhances the initial and final degradation temperatures of pure PW and PW/TiO_2 composites. This research shows the addition of TiO_2 nanoparticles improves the thermal stability of PW. The temperature at which deterioration begins for PW, PW/TiO_2-0.1, PW/TiO_2-0.5, PW/TiO_2-1.0 and PW/TiO_2-2.0 are 309.24 °C, 309.98 °C, 309.21 °C, 313.31 °C and 316.29 °C respectively.

The focal reduction temperature of PW/TiO_2-2.0 is found to be 325.25 °C, which shows a slight increment in the final degradation temperature of nanocomposite using TiO_2 with pure PW. At temperatures higher than pure paraffin PW, more excellent thermal stability is seen, whereas a lower value indicates a decrease in thermal stability [36]. The onset degradation temperature for binary composite by addition of Graphene nanoparticles with PW/TiO_2 composites PW/TiO_2-Gr-0.1, PW/TiO_2Gr-0.5, PW/TiO_2Gr-1.0 and PW/TiO_2Gr-2.0 are 315.90 °C, 316.44 °C, 320.22 °C and 325.25 °C respectively. With the addition of Graphene nanoparticles to NEOPCM composite, the thermal degradation occurs higher than the base PW. Admittedly, all deterioration temperatures are within 10 °C of the temperature of pure PW, indicating only a minor variance in the thermal degradation of binary composites that have been produced. It demonstrates that Graphene can improve the thermal stability of the RT47 PW base. Because the TiO_2-Graphene nanoparticles form a thermal barrier when heated, this may be what causes the improved thermal stability.

3.4. Thermal conductivity

Fig. 7(a) and (b) shows the thermal conductivity of PW, PW/TiO_2 and PW/TiO_2Gr composites, respectively. The measurement demonstrated the composite PCM's values PW, PW/TiO_2-0.1, PW/TiO_2-0.5, PW/TiO_2-1.0 and PW/TiO_2-2.0 are 0.1958 ± 0.019 W/mK, 0.3247 ± 0.032 W/mK, 0.3632 ± 0.036 W/mK, 0.4304 ± 0.043 W/mK, 0.3655 ± 0.036 W/mK, respectively. All samples show greater TC as related to base PW. Due to TiO_2's exceptionally high TC compared to PW, the composites' TC rose as the mass ratio of TiO_2 nanoparticles increased. SDBS was used as a surfactant to improve the TC of composites. TC has a significant effect on the pace at which energy is stored. It is seen in Fig. 7 (a) that the TC of PW/TiO_2 nanocomposite upsurge with the concentration of TiO_2 up to 1% and then decrease at PW/TiO_2-2.0. Results obtained at high concentrations imply that the samples are not stable. The agglomeration of nanoparticles changes the measuring region's composition and properties, resulting in thermal conductivities that are significantly nearby the base PCM. Since a result of this, efficacy is diminished, resulting in the collapse of the thermal network and decreased TC. [37].

In Fig. 7(b), since Graphene has a much higher TC than RT47 PCM, the TC of the binary composites PW/TiO_2Gr-0.1, PW/TiO_2Gr-0.5, PW/TiO_2Gr-1.0 and PW/TiO_2-2.0% increased as 0.2361, 0.2796, and 0.3491, which are 120.58%, 142.80% and 179.03% increment concerning base PW PCM. The measurement showed the composite PCM's values PW/TiO_2Gr-0.1, PW/TiO_2Gr-0.5, PW/TiO_2Gr-1.0 and PW/TiO_2Gr-2.0 are 0.4319 ± 0.043 W/mK, 0.475 ± 0.475 W/Mk, 0.544 ± 0.054 W/mK and 0.396 ± 0.039 W/mK, respectively. The addition of TiO_2, Graphene and SDBS led to an increase in the TC of the composites. All the nanocomposite shows a greater increment in the TC by adding TiO_2 and Graphene nanoparticles. PW/TiO_2Gr-1.0 showed the greater TC at 0.5441 ± 0.054 W/mK, which is an increment of ~179.03%. The amount of TiO_2 and Graphene in the composite PCM increased, and the TC increased dramatically. The TC of the composite PCMs with PWTiO_2-1.0 and PW/TiO_2Gr-1.0 is 2.20 times and 2.78 times, respectively than PW. The increase in TC by inserting nanoparticles into PCM is evident compared to introducing nanoparticles into base PW. The TC of composite enhances with concentration up to 1%, and then decrement trend is seen at PW/TiO_2-2.0 and PW/TiO_2Gr-2.0. The reduction of TC at higher concentrations is because of the agglomeration of nanoparticles [38]. That is the key reason for efficacy as it led to the breakdown of the thermal network and reduction in TC [39,40]. The enhancement in the TC for PW/$TiO_2$and PW/TiO_2Gr binary composite related to Paraffin may be ascribed to the improved thermal network within the PCM matrix due to highly conductive nanoparticles [41]. But as concentration increases above 1%, the agglomeration occurs, creating thermal breakdown and decreasing electron thermal transport. There are two types of thermal heat transfer mechanisms: electron transport and phonon transport. PW is based on phonon-phonon transport, which is similar to electron transport in metals and conducting polymers. Phonons are critical for heat transmission in materials. Generally, the

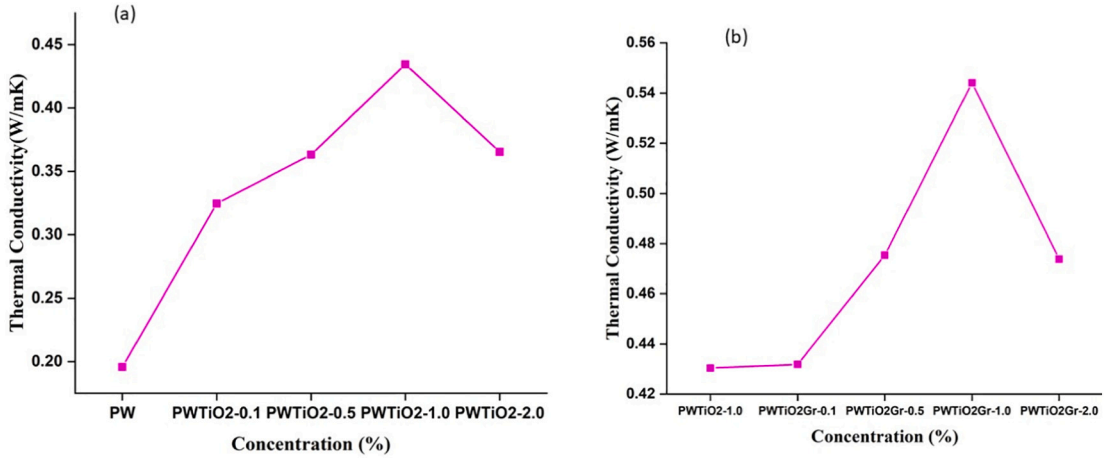

Fig. 7. The curves of thermal conductivity vs concentration (%) of PW, PW/TiO_2 in (a) and of PW/TiO_2Gr in (b).

greater the strength of phonon diffusion in a material, the greater its capacity to transfer heat and hence the higher its TC, and vice versa. The diverse phonon scatterings inside materials are the primary cause of phonon diffusion degradation. Phonon scattering may be classified into three types: phonon-phonon scattering, phonon-defect scattering, and phonon-interface scattering. [37]. In phonon transfer, the impurities develop more with concentration, increasing the phonon scattering impurities, resulting in a shorter mean free path and thus a decrease in TC. The reduction in TC of PW/TiO_2 and PW/TiO_2Gr-1.0 could result from a tradeoff between electron and phonon thermal transport. As a result, the optimal concentration for increased TC is PW/TiO_2-1.0 and PW/TiO_2Gr-1.0.

3.5. Chemical stability

The FT-IR study was done to see whether any chemical or physical reactions between the various components of the composites. The FT IR transmission spectrum of PW/TiO_2 NEOPCM and PW/TiO_2Gr binary composite are given in Fig. 8a and b correspondingly. Based on the current evidence, composite PW/TiO_2 exhibits four distinct transmission or absorption bands, as depicted in Fig. 8a: CH2 rocking vibration at 720 cm^{-1}, CH2 and CH3 deformation vibration at 1467 cm^{-1}, and intense peaks at 2850 cm^{-1} and 2917 cm^{-1}, which correspond to CH2—CH3 stretching vibrations [42] and intense peaks at 2850 cm^{-1} and 2917 cm^{-1}, respectively. When it comes to C—H stretching vibrations, the first two peaks correspond to the aliphatic and methyl groups. In contrast, the third peak corresponds to the deformation vibration of the —CH2 and —CH3 bond and the fourth peak corresponds to the rocking vibration of the —CH2 bond. PW and PW/TiO_2 composites designated as PW/TiO_2-0.1, PW/TiO_2-0.5, PW/TiO_2-1.0, and PW/TiO_2-2.0 were used to study the FTIR spectra at 4000–400 cm^{-1} frequencies and were shown to be effective. The PW and PW/TiO_2 composites have almost similar peak heights, and there is no evidence of a new peak. The existence of a similar peak indicates that the particle's additives and the surfactant are not reacting chemically and that only physical contact occurs. As shown in Fig. 6b, the main absorption peaks of composite PW/TiO_2Gr are 2917 cm^{-1}, 2850 cm^{-1}, 1467 cm^{-1}, and 720 cm^{-1}, respectively. The C—H2 bonding of the Paraffin has a peak at 2917 cm^{-1} and 2850 cm^{-1}, indicating that it is highly stable.

The peak defines the Paraffin contains the stable balance of attractive and repulsive forces between carbon and hydrogen atoms [43]. Due to C—H3 stretching vibration, oxygen functionalities were observed in the composite peaks 1467 cm^{-1} and 720 cm^{-1}. It is noticeable no new peaks are formed in both PW/TiO_2 composites preparation. Fig. 8b shows FT IR spectrum of PW, TiO_2 nanoparticles, Graphene nanoparticles and the composites PW/TiO_2-1.0, PW/TiO_2Gr-0.1, PW/TiO_2Gr-0.5, PW/TiO_2Gr-1.0 and PW/TiO_2Gr-2.0. Based on the current evidence, binary composites PW/TiO_2Gr have four distinct transmission or absorption bands the same as in the case of PW/TiO_2 composites. According to the current evidence, composite PW/TiO_2Gr displays four different transmission or absorption bands, as illustrated in Fig. 8b. CH2 rocking and deformation vibrations vary at 720 cm^{-1}, 1467 cm^{-1}, and 2850 cm^{-1}, respectively, which correspond to CH2—CH3 stretching vibrations. Intense peaks occur at 2850 cm^{-1} and 2917 cm^{-1}, which correspond to CH2—CH3 stretching vibrations [42].

Regarding stretching vibrations between atoms of the C—H bond, the first two peaks belong to the aliphatic and methyl groups, respectively. The third peak corresponds to deformation vibrations of the CH2 and —CH3 bonds, while the fourth peak refers to rocking vibrations of the —CH2 bond. In order to investigate the FTIR spectra at 4000–400 cm^{-1} frequencies, the PW/TiO_2 composites PW/TiO_2-0.1, PW/TiO_2-0.5, PW/TiO_2-1.0, and PW/TiO_2-2.0 were employed. The results showed that the composites were effective. The peak heights of the PW and PW/TiO_2Gr composites are virtually identical, and there is no indication of the formation of a new peak. The presence of a comparable peak shows that the particle's additives and the surfactant are not interacting chemically and that only physical contact is taking place between the two substances. Adding the SDBS to PW/TiO_2 composite and added Graphene

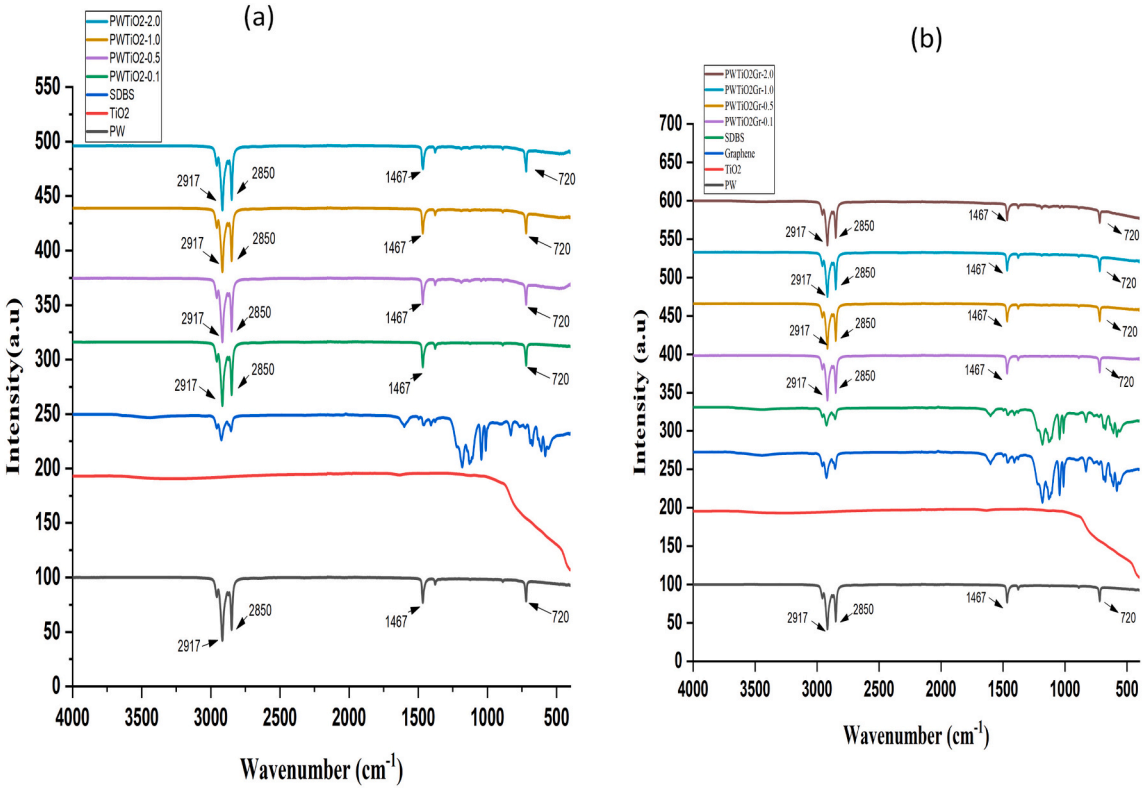

Fig. 8. FTIR Spectrum curves for intensity v/s wavenumber (cm^{-1}) of (a) PW/TiO_2 (b) PW/TiO_2Gr.

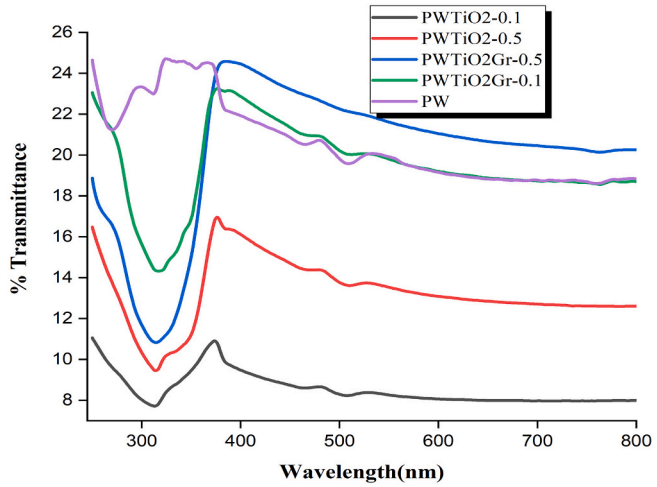

Fig. 9. Light transmission curve of PW/TiO_2 and PW/TiO_2Gr.

nanoparticles did not result in new peaks in the FTIR spectrum of PW/TiO_2Gr composite, as can be seen from Fig. 8b.

3.6. UV–Vis light transmission capability

The transmissibility of the UV–VIS spectra of PW/TiO_2 and PW/TiO_2Gr binary composites is depicted in Fig. 9. PW Base PCM, PW/TiO_2-0.1, PW/TiO_2-0.5, PW/TiO_2Gr-0.1, PW/TiO_2Gr-0.5 have transmittance of 19.81%, 16.53%, 12.50%, 10.35% and 8.30% respectively as compared with solar spectrum. The prepared composites reduced light transmission by 58.30% compared to pure PW; maximum reduction is due to the introduction of TiO_2 and Graphene nanoparticles into PW. The decrease in solar spectrum transmission indicates increased light absorption and, subsequently, enhanced photothermal conversion.

Results of the UV–VIS spectrum of the PW/TiO_2Gr binary composite show a reduction in the sample's transmissibility is accompanied by dispersion of nanoparticles in PW [44]. A maximum reduction in transmission of 36.90% is achieved with the PW/TiO_2 composite. The transmittance of PW/TiO_2 has been reduced by 33.2% compared with PW/TiO_2 composite. When the findings were compared, it was found that the PW/TiO_2Gr binary composite performs significantly better than the PW/TiO_2 in terms of direct light absorption. The enhanced absorptivity of the binary composite can be related to the Graphene nanoparticles' outstanding photothermal properties.

3.7. Thermal reliability

The Thermal cycling tests were conducted to confirm the prepared nano enhanced phase change material's (NePCMs) thermal reliability. The samples were placed in a custom-built thermal cycler equipped with three chambers to allow for simultaneous testing of three samples. The samples were placed in a crucible and an electronically controlled thermocouple was introduced into each one. The maximum temperature is kept at 65 °C, at least 10 °C above the melting point of the sample, to ensure full melting. To obtain the maximum temperature, the samples were heated from below the crucible holder. When the maximum temperature has been reached, the heater is auto turned off. This initiates the cooling cycle, during which the sample is cooled from above using a Peltier cooling system. The minimum temperature for the cooling cycle is kept as 25 °C. Due to the less quantity of sample size used, approximately 500 mg–800 mg, the maximum temperature is reached in 2 min, while the cooling cycle takes slightly longer, approximately 3 min. Thermal reliability was assessed for the PW, TiO_2 added composite, and binary composite using accelerated thermal cycler. The thermal cycling properties of paraffin and the selected composite are determined using TGA, DSC, and FTIR data taken at 0 and 300 cycles. Due to their high thermal conductivity values, two composites, PWTiO_2-1.0 and

Table 2
DSC data after 0 and 300 thermal cycles.

Composite	Latent heat J/g		Melting point °C	
	0 cycle	300 cycles	0 cycle	300 cycles
PW	145	142.29	48.77	47.0
PWTiO_2-1.0	121	116	48.61	47.1
PWTiO_2Gr-1.0	130	128	48.24	47.2

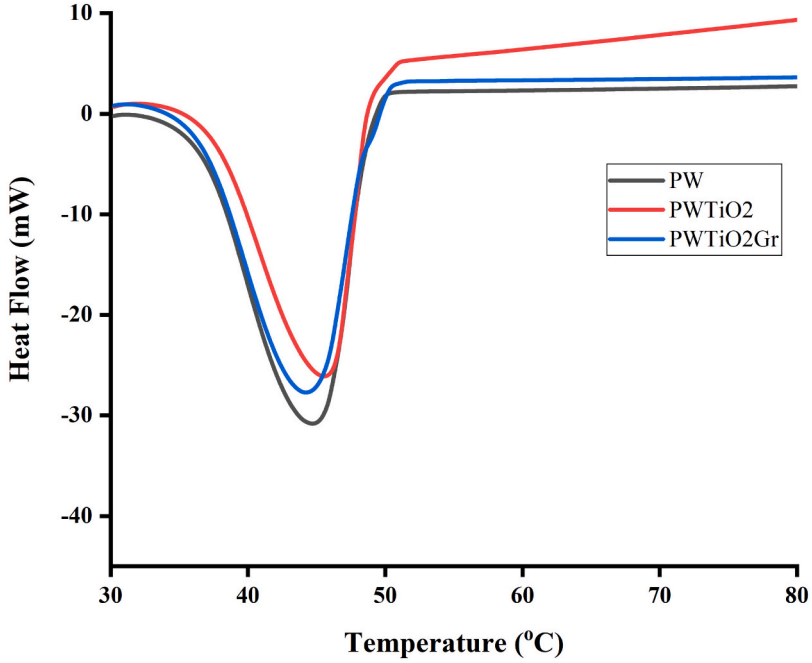

Fig. 10. DSC Curve of heat flow vs temperature 300 cycles PW, PW-TiO_2 and PW-TiO_2 Gr.

PWTiO$_2$Gr-1.0, were chosen for accelerated thermal cycling. Fig. 10 illustrates the DSC curve of thermally cycled paraffin wax PW, PW-TiO$_2$ and PW-TiO$_2$ Gr at 300 thermal cycles and the data is summarized in Table 2. At 300 thermal cycles, paraffin wax PW, PW-TiO$_2$ and PW-TiO$_2$ Gr has a latent heat storage capacity of 142.61 ± 3.07 J/g and 116.71 ± 2.91 J/g and 128.71 ± 2.91 J/g, respectively. Additionally, paraffin wax PWTiO$_2$-1.0 and PWTiO$_2$Gr-1.0 melted at 47.0 ± 0.2 °C, 48.1 ± 0.2 °C, and 48.2 ± 0.2 °C, respectively. The thermal cycled samples lack the solid-solid transition area, even if the solid-to-solid transition phase is not visible in the DSC curve, this may be owing to particle agglomeration caused by repeated phase changes may account for the decrease in latent heat at 300 cycles from 145.31 ± 2.90 J/g to 142.71 ± 2.84 J/g, 121 ± 2.42 J/g to 116.71 ± 2.32 J/g and 130 ± 2.60 J/g to 128 ± 2.56 J/g respectively. The percent decrease in performance is attributable to the faster thermal cycling.

The FT-IR analysis was performed to determine whether any chemical or physical reactions occurred between the composites' constituent components after 300 cycles. Fig. 11 illustrates the FTIR transmission spectra of 300 cycles PW, PW/TiO$_2$-1.0, and PW/TiO$_2$Gr-1.0 binary composites. Composite and PW display four same transmission or absorption bands, as illustrated in Fig. 11: CH2 rocking vibration at 720 cm^{-1}, CH2 and CH3 deformation vibration at 1467 cm^{-1}, and intense peaks at 2850 cm^{-1} and 2917 cm^{-1}, respectively, which correspond to CH2—CH3 stretching vibrations and intense peaks at 2850 cm^{-1} and 2917 cm^{-1}. The first two peaks correspond to the aliphatic and methyl groups, respectively, in terms of stretching vibrations between C—H bond atoms. The third peak relates to the deformation vibrations of the CH2 and —CH3 bonds, whereas the fourth peak belongs to the —CH2 bond rocking. The PW and composites were used to analyze the FTIR spectra at 4000–400 cm^{-1} frequencies. The composites were found to be effective. The peak heights of the 300 cycles PW, PWTiO$_2$ and PW/TiO$_2$Gr composites are almost comparable, and there is no evidence of a new peak forming. The decrease in intensity could have been due to particle agglomeration, whereas the new peak could be due to the development of a C═C.

The initial degradation temperature for PW, PW/TiO$_2$-1.0, and PW/TiO$_2$Gr-1.0 after 300 thermal cycles can be seen in Fig. 12 and are similar to the initial decomposition temperature of uncycled zero cycle. The maximal decomposition temperature of PW, PW/TiO$_2$-1.0, and PW/TiO$_2$Gr-1.0 after 300 thermal cycles are 317.0, 329.25 °C and 334.3 °C, which is higher than the of zero cycle of PW (309.32 °C), PW/TiO$_2$-1.0 (313.31 °C), and PW/TiO$_2$Gr-1.0 (320.22 °C) samples. This clearly demonstrates the chemical and thermal stability of the nanocomposite dispersed Paraffin, indicating that it can be applied for TES while overcoming paraffin's low thermal conductivity.

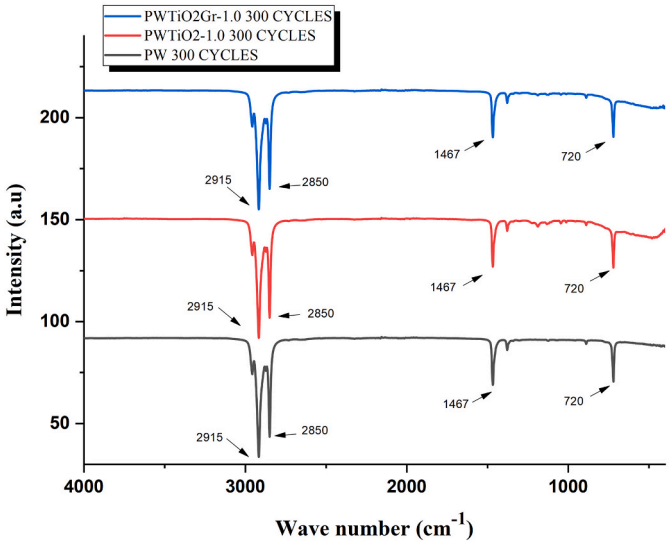

Fig. 11. FTIR Spectrum curves for intensity v/s wavenumber (cm^{-1}) of 300 cycles PW, PW/TiO$_2$ 1.0 and PW/TiO$_2$Gr-1.0.

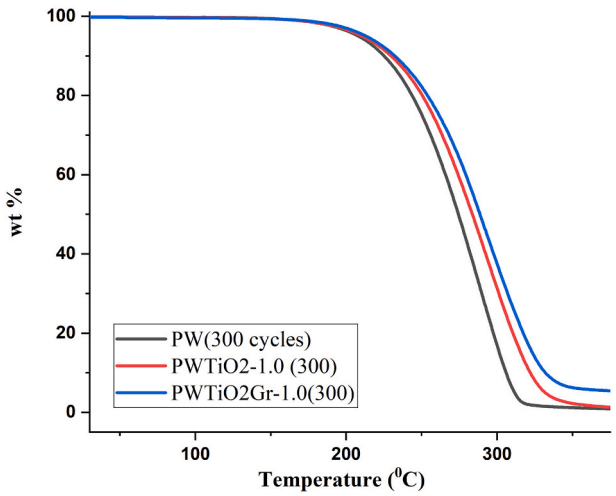

Fig. 12. TGA Curve of weight % vs temperature for 300 cycles PW, PW/TiO$_2$ 1.0 and PW/TiO$_2$Gr-1.0.

4. Conclusions

In this study, we determined the thermal behavior of the PW as PCM, PW/TiO$_2$ composite and PW/TiO$_2$Gr binary composite. The enhanced thermal characteristics of PW and composites were tailor-made via two-step preparation methods, commonly employed for TES. The characterization and thermophysical properties of the novel binary composite were explored; the FTIR study demonstrated no chemical interaction between the PW and the nanoparticles. Morphological characterization was done using FESEM and EDX to confirm imaging and observational spatial of all the elements. The EDX spectrum's peaks correspond to the elements carbon, oxygen, titanium, sodium and silver. Outcomes demonstrated that TiO$_2$ and Graphene are integrated into the paraffin matrix. The temperature and enthalpy of the melting and solidifying processes enhance the chemical and structural stability of the composites. The 0.1-PW/TiO$_2$ and the 0.1-PW/TiO$_2$Gr binary composite's latent heat capacity was improved by 8.62% and 10.02%, respectively. The TC shows a maximum increment of 120% (PW/TiO$_2$-1.0) and 179% (PW/TiO$_2$Gr-1.0) concerning base PCM. The obtained TGA results confirm that increment in the loading weight percentage of nanoparticles increases the thermal durability of the nanocomposite PW/TiO$_2$ and PW/TiO$_2$Gr. A thermophysical change in pure PW and NEOPCM composite was noted regarding initial and final degradation. The light transmission of the prepared composite was reduced by 58.30% related to base PW. All composite showed thermal degradation within 10 °C with compared to PW PCM. Thus, with the higher TC and enhanced thermal reliability, the PW/TiO$_2$ and PW/TiO$_2$Gr composites presented promising prospects for energy-efficient application of solar photovoltaic thermal, domestic hot water and cooling application of electric drives.

CRediT authorship contribution statement

Imtiaz Ali Laghari: Data Curation, Investigation, Formal analysis, Writing - Original Draft

M. Samykano: Validation, Review & Editing, Methodology, Supervision, Project administration

A K Pandey: Conceptualization, Methodology, Formal analysis, Validation, Supervision, Project administration

K. Kadirgama: Writing - Review & Editing, Supervision

Yogeshwar Nath Mishra: Validation, Writing - Review & Editing

Declaration of competing interest

The authors declare that they have no known competing financial interests or personal relationships that could have appeared to influence the work reported in this paper.

Acknowledgement

The authors would like to thank Universiti Malaysia Pahang (UMP) and Ministry of Higher Education, Malaysia for the financial support given under Fundamental Research Grant Scheme: FRGS/1/2021/STG05/UMP/02/5 and Sunway University through Sunway University's International Research Network Grant Scheme (IRNGS) 2021 (STR-IRNGS-SET-RCNMET-01-2021) for carrying out this research.

Data availability

Data will be made available on request.

References

[1] J.B. Smith, in: Assessing Dangerous Climate Change Through an Update of the Intergovernmental Panel on Climate Change (IPCC) "'Reasons for Concern,"' vol. 106, 2009, pp. 4133–4137, no. 11.
[2] O. Edenhofer, Accidents and risks BT - IPCC special report on renewable energy sources and climate change mitigation, in: IPCC Spec. Rep. Renew. Energy Sources Clim. Chang. Mitig., no. 9.3.4.7, 2011 [Online]. Available: papers2://publication/uuid/7656EAFA-9B72-48D8-B960-300B0C7A388A.
[3] K. Kant, A. Shukla, A. Sharma, Advancement in phase change materials for thermal energy storage applications, Sol. Energy Mater. Sol. Cells 172 (April) (2017) 82–92, https://doi.org/10.1016/j.solmat.2017.07.023.
[4] S.L. Tariq, H.M. Ali, M.A. Akram, M.M. Janjua, M. Ahmadlouydarab, Nanoparticles enhanced phase change materials (NePCMs)-a recent review, Appl. Therm. Eng. 176 (April) (2020) 115305, https://doi.org/10.1016/j.applthermaleng.2020.115305, 2019.
[5] L. Yang, F. Zhou, J.Nan Huang, Thermophysical properties and applications of nano-enhanced PCMs: an update review, Energy Convers. Manag. 214 (March) (2020) 112876, https://doi.org/10.1016/j.enconman.2020.112876.
[6] N. Jamil, et al., A review on nano enhanced phase change materials: an enhancement in thermal properties and specific heat capacity, J. Adv. Res. Fluid Mech. Therm. Sci. 57 (1) (2019) 110–120.
[7] H. Jouhara, A. Żabnieńska-Góra, N. Khordehgah, D. Ahmad, T. Lipinski, Latent thermal energy storage technologies and applications: a review, Int. J. Thermofluids 5–6 (2020), https://doi.org/10.1016/j.ijft.2020.100039.
[8] S. Wu, T. Yan, Z. Kuai, W. Pan, Thermal conductivity enhancement on phase change materials for thermal energy storage: a review, Energy Storage Mater. 25 (October) (2020) 251–295, https://doi.org/10.1016/j.ensm.2019.10.010, 2019.
[9] T. ur Rehman, H.M. Ali, Experimental study on the thermal behavior of RT-35HC paraffin within copper and Iron-Nickel open cell foams: energy storage for thermal management of electronics, Int. J. Heat Mass Transf. 146 (2020) 118852, https://doi.org/10.1016/j.ijheatmasstransfer.2019.118852.
[10] W.Q. Li, S.J. Guo, L. Tan, L.L. Liu, W. Ao, Heat transfer enhancement of nano-encapsulated phase change material (NEPCM) using metal foam for thermal energy storage, Int. J. Heat Mass Transf. 166 (2021), https://doi.org/10.1016/j.ijheatmasstransfer.2020.120737.
[11] A. Nematpour Keshteli, M. Sheikholeslami, Nanoparticle enhanced PCM applications for intensification of thermal performance in building: a review, J. Mol. Liq. 274 (2019) 516–533, https://doi.org/10.1016/j.molliq.2018.10.151.
[12] M.A. Kibria, M.R. Anisur, M.H. Mahfuz, R. Saidur, I.H.S.C. Metselaar, A review on thermophysical properties of nanoparticle dispersed phase change materials, Energy Convers. Manag. 95 (2015) 69–89, https://doi.org/10.1016/j.enconman.2015.02.028.
[13] G.V. Belessiotis, K.G. Papadokostaki, E.P. Favvas, E.K. Efthimiadou, S. Karellas, Preparation and investigation of distinct and shape stable paraffin/SiO2 composite PCM nanospheres, Energy Convers. Manag. 168 (April) (2018) 382–394, https://doi.org/10.1016/j.enconman.2018.04.059.
[14] K. B, Synthesis and characterization of conducting polyaniline@cobalt-Paraffin wax nanocomposite as nano-phase change material: enhanced thermophysical properties, Renew. Energy 173 (2021) 1057–1069, https://doi.org/10.1016/j.renene.2021.04.050.
[15] P. Kumar, P. Kumar Singh, S. Nagar, K. Sharma, M. Saraswat, Effect of different concentration of functionalized graphene on charging time reduction in thermal energy storage system, Mater. Today Proc. 44 (2020) 146–152, https://doi.org/10.1016/j.matpr.2020.08.548.
[16] H. Mhiri, A. Jemni, H. Sammouda, Numerical and experimental investigations of melting process of composite material (nanoPCM/carbon foam) used for thermal energy storage, J. Energy Storage 29 (December) (2020) 101167, https://doi.org/10.1016/j.est.2019.101167, 2019.
[17] J. Lin, Enhancing the solar absorption capacity of expanded graphite-paraffin wax composite phase change materials by introducing carbon nanotubes additives, Surf. Interfaces (2022) 101871, https://doi.org/10.1016/j.surfin.2022.101871.
[18] J. Yang, Y. Jia, N. Bing, L. Wang, H. Xie, W. Yu, Reduced graphene oxide and zirconium carbide co-modi fi ed melamine sponge/para ffi n wax composites as new form-stable phase change materials for photothermal energy conversion and storage, Appl. Therm. Eng. 163 (July) (2019) 114412, https://doi.org/10.1016/j.applthermaleng.2019.114412.
[19] M. Chen, Y. He, Q. Ye, Z. Zhang, Y. Hu, International journal of heat and mass transfer solar thermal conversion and thermal energy storage of CuO / paraffin phase change composites, Int. J. Heat Mass Transf. 130 (2019) 1133–1140, https://doi.org/10.1016/j.ijheatmasstransfer.2018.11.026.
[20] H. Masoumi, R. Haghighi, S.M. Mirfendereski, Thermochimica acta modification of physical and thermal characteristics of stearic acid as a phase change materials using TiO 2-nanoparticles, Thermochim. Acta 675 (February) (2019) 9–17, https://doi.org/10.1016/j.tca.2019.02.015.
[21] M.S. Kumar, V.M. Krishna, Experimental investigation on performance of hybrid PCM's on addition of nano particles in thermal energy storage, Mater. Today Proc. 17 (2019) 271–276, https://doi.org/10.1016/j.matpr.2019.06.430.
[22] X. Sun, L. Liu, Y. Mo, J. Li, C. Li, Enhanced thermal energy storage of a paraffin-based phase change material (PCM) using nano carbons, Appl. Therm. Eng. 181 (July) (2020), 115992, https://doi.org/10.1016/j.applthermaleng.2020.115992.
[23] P. Manoj Kumar, K. Mylsamy, P.T. Saravanakumar, R. Anandkumar, A. Pranav, Experimental study on thermal properties of Nano-TiO2 embedded paraffin (NEP) for thermal energy storage applications, Mater. Today Proc. 22 (2019) 2153–2159, https://doi.org/10.1016/j.matpr.2020.03.282.
[24] N. Aslfattahi, Improved thermo-physical properties and energy efficiency of hybrid PCM/graphene-silver nanocomposite in a hybrid CPV/thermal solar system, J. Therm. Anal. Calorim. (0123456789) (2020), https://doi.org/10.1007/s10973-020-10390-x.
[25] A.O. Elsayed, Numerical study on performance enhancement of solid-solid phase change materials by using multi-nanoparticles mixtures, J. Energy Storage 4 (2015) 106–112, https://doi.org/10.1016/j.est.2015.09.008.
[26] I.A. Laghari, M. Samykano, A.K. Pandey, K. Kadirgama, V.V. Tyagi, Advancements in PV-thermal systems with and without phase change materials as a sustainable energy solution: energy, exergy and exergoeconomic (3E) analytic approach, Sustain. Energy Fuels 4 (10) (2020) 4956–4987, https://doi.org/10.1039/d0se00681e.
[27] R. Reji Kumar, M. Samykano, A.K. Pandey, K. Kadirgama, V.V. Tyagi, Phase change materials and nano-enhanced phase change materials for thermal energy storage in photovoltaic thermal systems: a futuristic approach and its technical challenges, Renew. Sust. Energ. Rev. 133 (April) (2020), 110341, https://doi.org/10.1016/j.rser.2020.110341.
[28] K. Du, J. Calautit, Z. Wang, Y. Wu, H. Liu, A review of the applications of phase change materials in cooling, heating and power generation in di ff erent temperature ranges, Appl. Energy 220 (October) (2018) 242–273, https://doi.org/10.1016/j.apenergy.2018.03.005, 2017.
[29] J. Jaguemont, N. Omar, P. Van Den Bossche, J. Mierlo, Phase-change materials (PCM) for automotive applications : a review, Appl. Therm. Eng. 132 (2018) 308–320, https://doi.org/10.1016/j.applthermaleng.2017.12.097.
[30] D. Li, et al., Influence of morphology and interfacial interaction of TiO2-graphene nanocomposites on the visible light photocatalytic performance, J. Solid State Chem. 286 (January) (2020), 121301, https://doi.org/10.1016/j.jssc.2020.121301.
[31] D. Nanorod, "TiO2 / Graphene TiO2 / Graphene.".
[32] J. Wang, H. Xie, Z. Guo, L. Guan, Y. Li, in: Improved Thermal Properties of Paraf fi n Wax by the Addition of TiO 2 Nanoparticles vol. 73, 2014, pp. 1541–1547, https://doi.org/10.1016/j.applthermaleng.2014.05.078.
[33] F. Bahiraei, A. Fartaj, G. Nazri, Experimental and numerical investigation on the performance of carbon- based nanoenhanced phase change materials for thermal management applications, Energy Convers. Manag. 153 (October) (2017) 115–128, https://doi.org/10.1016/j.enconman.2017.09.065.
[34] L. Colla, L. Fedele, S. Mancin, L. Danza, O. Manca, Nano-PCMs for enhanced energy storage and passive cooling applications, Appl. Therm. Eng. 110 (2017) 584–589, https://doi.org/10.1016/j.applthermaleng.2016.03.161.
[35] J.L. Zeng, et al., Myristic acid/polyaniline composites as form stable phase change materials for thermal energy storage, Sol. Energy Mater. Sol. Cells 114 (2013) 136–140, https://doi.org/10.1016/j.solmat.2013.03.006.
[36] H. Masoumi, R. Haghighi Khoshkhoo, S.M. Mirfendereski, Modification of physical and thermal characteristics of stearic acid as a phase change materials using TiO 2-nanoparticles, Thermochim. Acta 675 (February) (2019) 9–17, https://doi.org/10.1016/j.tca.2019.02.015.
[37] M. George, A.K. Pandey, N. Abd Rahim, V.V. Tyagi, S. Shahabuddin, R. Saidur, A novel polyaniline (PANI)/paraffin wax nano composite phase change material: superior transition heat storage capacity, thermal conductivity and thermal reliability, Sol. Energy 204 (February) (2020) 448–458, https://doi.org/10.1016/j.solener.2020.04.087.
[38] N. Navarrete, et al., Thermal energy storage of molten salt based nanofluid containing nano-encapsulated metal alloy phase change materials, Energy (2018), https://doi.org/10.1016/j.energy.2018.11.037.
[39] Y. Zhou, et al., Multifunctional ZnO/polyurethane-based solid-solid phase change materials with graphene aerogel, Sol. Energy Mater. Sol. Cells 193 (January) (2019) 13–21, https://doi.org/10.1016/j.solmat.2018.12.041.

[40] S. Wu, T. Yan, Z. Kuai, W. Pan, Thermal conductivity enhancement on phase change materials for thermal energy storage: a review, Energy Storage Mater. 25 (September) (2020) 251–295, https://doi.org/10.1016/j.ensm.2019.10.010, 2019.
[41] D. Li, et al., Effect of MOF derived hierarchical Co3O4/expanded graphite on thermal performance of stearic acid phase change material, Sol. Energy 171 (December) (2018) 142–149, https://doi.org/10.1016/j.solener.2018.06.062, 2017.
[42] N. Mekaddem, S. Ben Ali, M. Fois, A. Hannachi, Paraffin/expanded perlite/plaster as thermal energy storage composite, Energy Procedia 157 (2019) 1118–1129, https://doi.org/10.1016/j.egypro.2018.11.279.
[43] V. Allahyarzadeh, M. Montazer, N.H. Nejad, N. Samadi, In situ synthesis of nano silver on polyester using NaOH/Nano TiO 2, J. Appl. Polym. Sci. 129 (2) (2013) 892–900, https://doi.org/10.1002/app.38907.
[44] C.A. Gueymard, The sun's total and spectral irradiance for solar energy applications and solar radiation models, Sol. Energy 76 (4) (2004) 423–453, https://doi.org/10.1016/j.solener.2003.08.039.